JOURNAL OF CATALYSIS 132, 157–182 (1991)

Catalytic Cooperation between MoO_3 and Sb_2O_4 in N-Ethyl Formamide Dehydration

I. Preparation, Characterization, and Catalytic Results

BING ZHOU,[1] EDGARDO SHAM, TADEUSZ MACHEJ,[2] PATRICK BERTRAND,[3] PATRICIO RUIZ, AND BERNARD DELMON

Catalyse et Chimie des Matériaux Divisés, Université Catholique de Louvain, Place Croix du Sud 1, 1348 Louvain-la-Neuve, Belgium

Received January 19, 1990; revised March 27, 1991

Catalysts containing MoO_3 and α-Sb_2O_4 with different "architectures" were prepared by different methods: mixing of separately prepared pure oxides, impregnation of MoO_3 by Sb_2O_4 or vice versa. We report results obtained in the oxygen-aided dehydration of N-ethyl formamide catalyzed by these solids. A strong synergy between Mo and Sb is always observed. Extensive characterization of the catalysts before and after catalytic test, by X-ray diffraction, Electron Microscopy, Analytical Electron Microscope, XPS, and Ion Scattering Spectroscopy excludes the formation of mixed oxides or solid solutions as well as mutual contamination. Rather, the artificial contamination created by impregnation with a precursor of the other oxide exhibits a strong tendency to disappear. The catalytic synergy persists after the contamination has disappeared. The origin of the observed synergy is attributed to a remote control mechanism, namely spillover oxygen produced by α-Sb_2O_4 creates and/or regenerates active and selective sites on MoO_3.

1. INTRODUCTION

Research previously carried out in this laboratory (*1–4*) has shown that N-ethyl formamide dehydration can be used as a test reaction for the understanding of the reaction mechanism of selective oxidation. The presence of several elements (and several phases) is necessary in good selective oxidation catalysts (multicomponent catalysts) (*5–15*). Because of the similitude of composition of catalysts active in formamide dehydration and in selective oxidation and of the surprising intervention of oxygen in the first reaction, we have conducted a program aimed at the study of the synergetic effects between catalyst components in the first reaction. We thus hoped to contribute to the understanding of the cooperation effects of the various elements in the second reaction.

The catalysts for selective oxidation of hydrocarbons have been reviewed by many authors (*5–14*). Among the elements present in these catalysts, molybdenum and antimony oxides play a very important role. In particular, it has been proposed that there exist correlations between catalytic and surface properties of catalysts containing pure MoO_3 (*1, 9, 11–13, 15, 16*) or Sb_2O_4 (*5, 10, 12, 17–21*). However, very few reports in the literature have been devoted to the study of mixed MoO_3 and Sb_2O_4 oxides. This is the first reason for the choice of these oxides for the present study.

In addition, MoO_3 and α-Sb_2O_4 constitute an ideal catalytic system for studying synergy: isolated α-Sb_2O_4 gives a negligible conversion of N-ethyl formamide, but, when in contact with MoO_3, a conspicuous increase of activity, compared to the simple addition of the activities of isolated oxides, is observed.

[1] Present Address: Dalian Institute of Chemical Physics, P.O. Box 110, Dalian, P.R. China.

[2] On leave from the Institute of Catalysis and Surface Chemistry, Polish Academy of Sciences, Cracow, Poland.

[3] Unité de Physico-Chimie et de Physique des Matériaux, Université Catholique de Louvain, Belgium.

0021-9517/91 $3.00

An observed synergistic effect in a system composed of two (or several phases) may be due to one or several of the following possibilities:

1. bi-functional catalysis,
2. remote control mechanism (*1–4*),
3. the formation of a solid solution or a mixed phase (compound oxide),
4. contamination of one phase by elements coming from the other,
5. formation of a monolayer (or epitaxial layers) of one phase on the surface of another.

For dehydration of N-ethyl formamide to propionitrile catalysed by a mixture of different phases, classical bifunctional catalysis can be ruled out on the basis of the very low stability of the only possible intermediary product, namely an isonitrile, the desorption of which from one phase, for absorption and further reaction on the other phase, seems extremely unlikely (*1*).

In the $MoO_3 + \alpha\text{-}Sb_2O_4$ system, the formation of any Mo–Sb–O mixed phase or a solid solution seems to be very difficult. Literature dealing with the formation of compounds such as $Sb_2(MoO_4)_3$, Sb_2MoO_6, etc. show that these compounds get easily decomposed into MoO_3 and $\alpha\text{-}Sb_2O_4$ (*22–25*).

If we suppose that MoO_3 and $\alpha\text{-}Sb_2O_4$ do not react with each other and do not suffer mutual contamination, the catalytic synergy between them could be well explained by a remote control mechanism (*1–4*). According to this mechanism, the active sites situated on the controlled phase (here MoO_3) would be created or regenerated by a spillover oxygen species emitted by the controlling phase (in this case $\alpha\text{-}Sb_2O_4$).

The main alternative explanation of the catalytic synergy by remote control might be contamination of one phase by elements from the other (namely possibilities 4 and 5).

The aim of our work was to study the reason for the synergistic effects observed with the molybdenum–antimony system. The results will be reported in a series of three papers.

The first one presents the detailed preparation, characterization, and catalytic results obtained with different types of catalysts. The following methods were used for preparation: (i) mechanical mixture of separately prepared oxides. In this case the contamination between the oxides is minimized and the oxides are in simple physical contact; (ii) impregnation of one oxide by small quantities of the metal of the other in order to facilitate the contamination between the oxides or even, if possible, form monolayers of the contaminating element on the other oxide; and (iii) co-precipitation of both oxides and/or calcination at high temperatures in order to maximize the conditions necessary to form a mixed oxide or a solid solution.

In order to study the modification in the solid state during the catalytic reaction, the samples were characterized before and after N-ethyl formamide dehydration by using a combination of different physico-chemical characterization techniques.

The principal conclusion of this work, as presented in this paper, was that a remote control mechanism could explain the synergism observed between MoO_3 and Sb_2O_4.

To give further support to this mechanism, it was essential to investigate also the nature of the active sites and the role played by spillover oxygen. The corresponding results will be reported in the second paper of this series.

In the third paper, the control effect of $\alpha\text{-}Sb_2O_3$ on the activity and selectivity of MoO_3 will be described qualitatively by using a mathematical model which takes into account all the parameters related to the remote control mechanism.

2. EXPERIMENTAL METHODS

2.1. Catalyst Preparation

2.1.1. Preparation of Pure Oxides

Used reagents were $(NH_4)_6Mo_7O_{24} \cdot 4H_2O$, Merck (pure grade with Fe < 0.0005%, Pb < 0.001%, and Cu < 0.001%), and Sb_2O_3, Merck (pure grade, with As < 0.005%, Ca < 0.002%, Cu < 0.002%, Fe <

0.003%, Pb < 0.002%, K < 0.002%, and Na < 0.002%).

MoO_3 (2.0 $m^2 g^{-1}$) was obtained by thermal decomposition of $(NH_4)_6Mo_7O_{24} \cdot 4H_2O$ in air at 500°C for 20 h.

Several α-Sb_2O_4 of different surface areas were prepared. Samples with surface areas of 0.4 and 2.0 m^2g^{-1} were obtained from calcination of Sb_2O_3 (Merck, p.a.) in air at 800°C for 100 h and 500°C for 20 h, respectively. Another sample of 5.2 $m^2 g^{-1}$ was obtained by using the oxidation method (*26*). Sb_2O_3 was oxidized by HNO_3 (UCB, 65%, p.a.) during 1 h at 50°C in a rotary evaporator under continuous stirring. After evaporation of the acid under a pressure lower than 1 atm, the solid was washed, filtered with distilled water until pH = 6, and then dried in air at 80°C for 20 h. The calcination was performed at 450°C in air during 20 h.

2.1.2 Preparation of Mechanical Mixtures of the Oxides in Physical Contact (Ms)

The pure MoO_3 and α-Sb_2O_4 were dispersed in the *n*-pentane (Merck, p.a.). The suspension of solids was stirred in an ultrasonic vibrator Bransonic 32 during 10 min. The evaporation of *n*-pentane was performed under continued agitation at 25°C under a pressure lower than 1 atm until the suspension became solid. The remaining *n*-pentane was removed by drying in air at 80°C during 20 h.

The composition of the powder mixtures was expressed by the weight ratio $r = W_{MoO_3}/(W_{MoO_3} + W_{\alpha\text{-}Sb_2O_4})$. Samples of compositions varying from $r = 0.0$ to $r = 1.0$ were prepared.

The pure oxides ($r = 0$ and $r = 1$) were subjected to the same treatment with *n*-pentane as the mixtures.

2.1.3. α-Sb_2O_4 Impregnated by Mo (*MoiSb*)

The impregnation with molybdenum oxalate was chosen in an attempt to form a monolayer catalyst. According to literature (*27, 28*), the use of molybdenum oxalate is very efficient for deposition of a monolayer of MoO_3 on supports.

The precursor, molybdenum oxalate, was prepared by the following method: 35 g of $(NH_4)_6Mo_7O_{24} \cdot 4H_2O$ were added to a solution of 28 g oxalic acid in 130 ml distilled water maintained at 40°C. The water was removed by evaporation under continuous stirring and reduced pressure at 70°C. The resulting solid was dried overnight at 90°C.

The amount of MoO_3 corresponding to a monolayer coverage on the surface of α-Sb_2O_4 (2.0 $m^2 g^{-1}$) was calculated on the assumption that one molecule of MoO_3 covered about 0.17 nm^2 (*29*). The result was 0.3 wt%. The quantities of the precursor required to form respectively 0, $\frac{1}{4}$, $\frac{1}{2}$, 1, 2, and 4 layers of MoO_3 on the surface of 10 g of α-Sb_2O_4 were dissolved in 100 ml distilled water. The α-Sb_2O_4 powder was immersed in this solution. After 6 h of impregnation at 60°C in a rotary evaporator, the water was evaporated under a pressure lower than 1 atm. The sample obtained was dried at 120°C for 24 h and calcined at 430°C for 1 h. The reference sample with no Mo (α-Sb_2O_4) was subjected to the same succession of treatments as the impregnated samples.

2.1.4. MoO_3 Impregnated by Sb (SbiMo)

The reaction of the antimony chlorides with the hydroxylated MoO_3 was used to prepare these catalysts (*28, 30*).

The precursor was prepared by dissolution of 4.016 g $SbCl_5$ (Aldrich chemie, 99%) and 3.069 g $SbCl_3$ (Aldrich chemie, 99.5%) in 250 ml $CHCl_3$ (UCB, p.a.).

Ten grams of MoO_3 was first hydroxylated with 200 ml distilled water and then dried at 80°C for 8 h. It was considered that one molecule of α-Sb_2O_4 covered about 0.16 nm^2; this value was calculated from the structure of α-Sb_2O_4 (*31*). The calculated amount of α-Sb_2O_4 corresponding to a monolayer coverage on the MoO_3 (2.0 $m^2 g^{-1}$) was 0.64 wt%. The quantity of the precursor required to form respectively $\frac{1}{4}$, $\frac{1}{2}$, 1, 2, and 4 layers (as well as 0: reference pure MoO_3 sample) of α-Sb_2O_4 on the surface of

10 g of MoO_3 was diluted in 100 ml of $CHCl_3$. MoO_3 was immersed in the solution in a rotary evaporator under stirring at 25°C for 6 h. The sample was dried at 120°C for 15 h and calcined at 450°C for 1 h. The reference sample with no Sb(i.e., MoO_3) was subjected to the same succession of treatments as the impregnated catalysts.

2.1.5. Shorthand Designation of the Impregnated Samples

Mo and Sb contents are expressed as percentages of the MoO_3 or Sb_2O_4 weight to the support weight, respectively, and are designated as MoiSb wt% and SbiMo wt%.

2.1.6. Attempts to Prepare Solid Solutions or Mixed Phases

(*a*) *Solid state synthesis* (S_s). The sample was prepared by calcination in air at 600°C for 20 h of what we had referred to as standard mixture (Ms) of the oxides (Paragraph 2.1.2).

(*b*) *Coprecipitation by evaporation of aqueous solutions* (*Cs*). First, 4.45 g of $(NH_4)_6\ Mo_7O_{24} \cdot 4H_2O$ (Merck, p.a.) and 3.68 g of $SbCl_3$ (Aldrich Chemie 99.9%) were added to a 2.5 *M* HCl (UCB, 37% p.a.) solution. The volume of the solution was 250 ml. After the two solids were dissolved, the solution was evaporated under a pressure lower than 1 atm in a rotary evaporator. The temperature was kept constant at 60°C using a thermostat. After 2 h of precipitation, the solid residue was then washed, filtered with distilled water, and dried at 100°C in air for 24 h. The calcination was performed in air at 600°C for 20 h.

2.2. Catalytic Activity Measurements

Catalytic activities were measured in a conventional flow apparatus. The reactor was a glass tube (int. diameter: 4 mm). All connections were heated to avoid condensation of formamide or nitrile. The catalytic bed was maintained between two layers of quartz wool.

N-ethyl formamide was fed by saturation of a carrier gas passing through a saturator and a condenser held at 90 and 85°C, respectively. The carrier gas was the desired mixture of He (99.995%, l'Air Liquide belge) and O_2 (99.995%, l'Air liquide belge). No other reagent was fed.

Reaction products were analysed by "online" gas chromatography (Intersmat IGC 120 ML) with a Porapak Q column (2 m, 200°C).

130 mg of sample were used as catalyst. N-ethyl formamide pressure P_f was maintained at 6 Torr and oxygen pressure P_{O_2} varied from 0.3 to 45 Torr. Total pressure was 760 Torr (100 kPa). We used fresh catalysts for each experiment. Reproducibility of activity measurements were 7% (relative to the overall value).

Total gas hourly space velocity was 40,000 h^{-1}, liquid hourly space velocity was estimated to be 1.7 h^{-1}. Reaction temperatures T_R were selected in the range from 350 to 390°C. The standard reaction conditions were the following: P_f = 6 Torr, P_{O_2} = 15 Torr, and T_R = 370°C.

Products were propionitrile, acetonitrile, water, and CO_2. Propionitrile formation was the main reaction. In the presence of oxygen, more than 96% of the introduced carbon was in the products on a Mo1.0 sample. The reaction is presented in Eq. (1).

In the absence of oxygen, the reaction products were the same but the propionitrile yield decreased and CO_2 increased markedly. After 8 h, CO_2 became the main product and carbon balance was ca. 89% on a Mo1.0 sample.

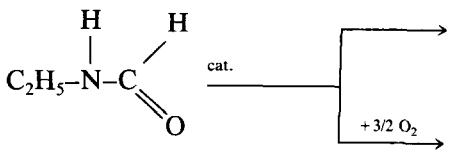

N-ethyl formamide

$C_2H_5{-}C{\equiv}N + H_2O$
Propionitrile

$CH_3{-}C{\equiv}N$
Acetonitrile $+2H_2O + CO_2$. (1)

We have checked that propionitrile, fed in the same conditions (with or without oxygen), does not react measurably.

Catalytic activities were expressed as yields (Y, %), namely propionitrile moles reported to the initial formamide moles fed into the catalytic bed; selectivities (S, %) were calculated from the equation $S = Y/C$, where conversion (C, %) was the total percentage of formamide transformed.

2.3. Characterization Techniques

BET surface areas were measured by N_2 adsorption at 77 K.

X-ray diffraction (XRD) was carried out with a Ni-filtered Cu Kα radiation.

Electron Spin Resonance (ESR) spectra were recorded by an X-band Varian-E12 spectrometer using 100 kHz modulation frequency and 20 mW incident microwave power. A detailed description of the measurements has been published elsewhere (*1c*).

The electron microscope used for analysis was a Jeol Temscan 100 Cx which enables the examination of the samples in the modes of scanning transmission (STEM), secondary electron scanning (SEM), and conventional transmission (CTEM). The instrument is also equipped with a Kevex 5100 C energy dispersive X-ray microanalyzer, which permits analytical electron microscopy measurements (AEM).

X-ray photoelectron spectroscopy (XPS) spectra were taken in a Vacuum Generator ESCA-3 MK II Spectrometer. The exciting radiation was Mg Kα (1253.6 eV). The C_{1s} line of carbon was used as the reference of binding energy (285 eV). A silica sample was used as an external reference for calculating the relative concentration $I_{rel}(M) = I_M/I_{Si2p}$ (M is $Sb3d_{3/2}$ or Mo3d) which was used in order to compare the composition of the XPS-analyzed portion (a near surface layer of a few nanometers in thickness) of the different samples. We shall call $I_{rel}(M)$ the relative analyzed concentration.

Ion Scattering Spectroscopy (ISS) measurements were carried out with a Kratos Spectrometer (Wg 541-515) which has been described elsewhere (*1b, 2*). In order to compare the different measurements, the peak areas were divided by the initial current density (I_0); the times of bombardment (t) were converted into ion dose (or fluence) (F) by: $F = I_0 \times t/1.6 \times 10^{-19}$, F in ions/cm^2, I_0 in A/cm^2, t in seconds. In order to quantify the surface composition of the samples, the calibration experiments were performed in the following manner: The spectra of the samples were compared with those containing only MoO_3 (sample $r = 1.0$) or α-Sb_2O_4 (sample $r = 0.0$) which has been treated under the same conditions as the samples, taken as standards. The surface composition can be deduced from the ratios of the Mo (or Sb) intensities in the sample and in the standard $r = 1.0$ (or $r = 0.0$).

From the literature, the sputtering yield (Y) for a metal with Ne^+ (2 keV) is about 1 (sputtered particle/incident ion) (*32*). It can be supposed (*33*) that the sputtering yields for an oxide are similar to those of the corresponding metal. The number of sputtered monolayers, N_m, with an ion dose F (ions/cm^2) can be calculated by $N_m = F\ Y/n_i$ (where n_i is the surface density of the oxide). Taking $n_{Sb_2O_4} = 1.67 \times 10^{15}$ (atom/cm^2) and $n_{MoO_3} = 1.83 \times 10^{15}$ (atom/cm^2), respectively, it can be estimated that an ion dose of approximately 2×10^{15} ions/cm^2 is required to remove one monolayer under our conditions of bombardment.

Analysis of carbon deposited on the catalysts was performed with a method proposed by Jones *et al.* (*34*).

3. RESULTS

3.1. Catalytic Activity of Mechanical Mixtures (Ms Samples)

Figure 1 presents the yields of Ms samples containing α-Sb_2O_4 of different surface areas (see caption) as a function of their mass ratio. Each activity curve passes through a maximum. The value of maximum yield does not change much. However, a displacement in the position of the maximum is observed. This displacement is always such that the overall surface area de-

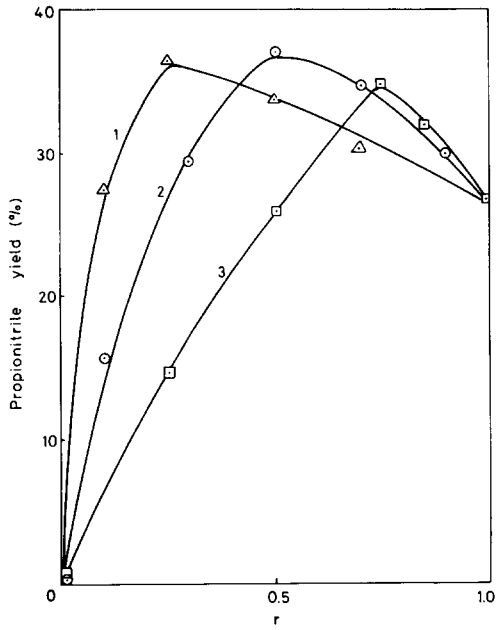

FIG. 1. Propionitrile yield as a function of mass ratio of Ms mixture containing MoO_3 (2.0 $m^2 g^{-1}$) and α-Sb_2O_4 ($m^2 g^{-1}$): (1) 0.4, (2) 2.0, and (3) 5.2, under standard conditions. Data taken at 5 min of time-on-stream.

veloped by the quantity of α-Sb_2O_4 in the mixture is comparable to that developed by MoO_3.

The Ms samples with MoO_3 ($2m^2 g^{-1}$) and α-Sb_2O_4 ($2m^2 g^{-1}$) were chosen for more detailed studies.

Figure 2 presents the propionitrile yield as a function of reaction time. Ms0.0 is not active. Ms1.0 has a marked activity in propionitrile yield, but this decreases during the reaction. The Ms0.5 sample, in which the MoO_3 and α-Sb_2O_4 are present together, gives a much higher propionitrile yield than Ms1.0. This yield does not change with time.

The selectivities of Ms0.5 and Ms1.0 samples correspond to about 95% propionitrile. They remain identical in the course of the reaction.

The yields as a function of the oxygen pressure at 8 h of reaction time are presented in Fig. 3.

The Ms0.0 sample is inactive in the whole range of oxygen pressure.

For the Ms1.0 sample, the yield increases with oxygen pressure from 0.3 to 45 Torr. We noted that the deactivation at low oxygen pressure was more pronounced than that at high oxygen pressure.

For the Ms0.5 sample, the yield increases with the oxygen pressure from 0.3 to 6 Torr. It reaches a plateau when the oxygen pressure is higher than 6 Torr. The yield of propionitrile for Ms0.5 is higher than for Ms1.0.

In all cases, propionitrile selectivities for the $r = 0.5$ and 1.0 samples did not change with the oxygen pressure and remained at about 95%. A small quantity of oxygen can maintain the selectivity.

In order to follow the deactivation of pure MoO_3 and a two-phase catalyst, reactions at 360°C with 6 Torr of N-ethyl formamide in the absence of oxygen during 8 h were carried out. The reaction results for Ms0.5 and Ms1.0 are presented in Table 1 (the Ms0.0 sample was not active).

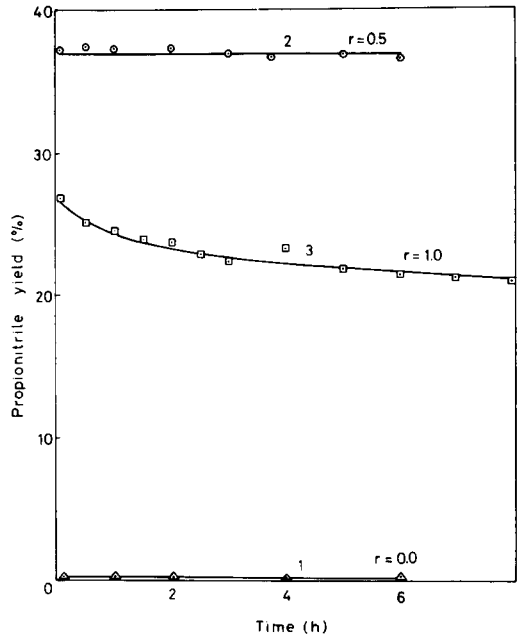

FIG. 2. Propionitrile yield as a function of reaction time under the standard reaction conditions for (1) Ms0.0 (pure α-Sb_2O_4), (2) Ms0.5, and (3) Ms1.0 (pure MoO_3).

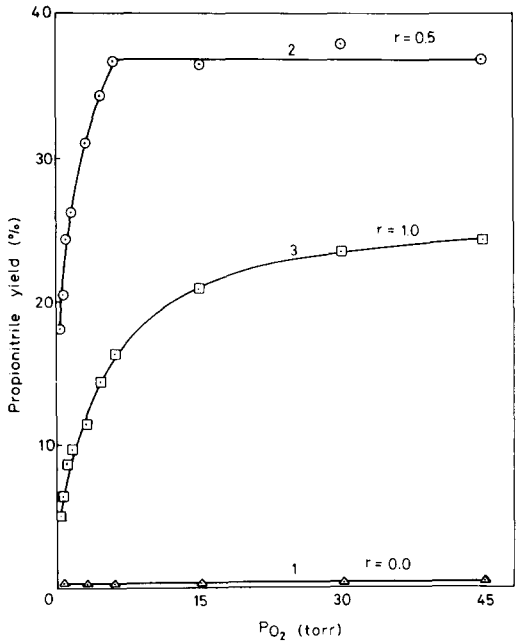

FIG. 3. Propionitrile yield as a function of oxygen partial pressure at 370°C with P_f = 6 Torr, after 8 h of reaction, for Ms samples: (1) r = 0.0 (pure α-Sb_2O_4), (2) r = 0.5, and (3) r = 1.0 (pure MoO_3).

TABLE 1

N-Ethyl Formamide Conversion (C, %) and Propionitrile Selectivity (S%) at 360°C with P_f = 6 Torr and P_{O_2} = 0 Torr during 8 h of Reaction

Samples		Reaction time (h)		
		0.0	0.5	8.0
Ms0.5	C %	28.3	11.9	11.2
	S %	76.9	61.6	10.3
Ms1.0	C %	20.2	30.1	15.2
	S %	73.7	21.9	11.5

For the Ms0.5 sample, the conversion decreased rapidly but selectivity remained fairly good after 0.5 h. For the Ms1.0 sample, the conversion increased after the first 0.5 h and then decreased, but selectivity decreased rapidly. After 8 h, the conversion and selectivity of both Ms0.5 and Ms1.0 samples decreased to a low value.

3.2. Catalytic Activity of Impregnated Catalysts

3.2.1. Activity of MoiSb Samples (α-Sb_2O_4 Impregnated by Mo)

The evolution of the propionitrile yield as a function of the reaction time is presented in Fig. 4. MoiSb0.0% is not active, but impregnation with a small amount of Mo gives samples producing a high yield of propionitrile. A conspicuous increase of yield with the increase of the MoO_3 contents is observed. For the samples containing 0.075, 0.15, and 0.3 wt% of MoO_3, the yields decrease during the first 1.5 h of reaction time. For those containing 0.6 and 1.2 wt% of MoO_3, the yields remain stable. The propionitrile yield of all samples stabilizes after 1.5 h of reaction.

The propionitrile selectivity does not change with the reaction time. Increasing the MoO_3 contents from 0.075 to 0.6 wt% decreases the selectivity from about 100 to

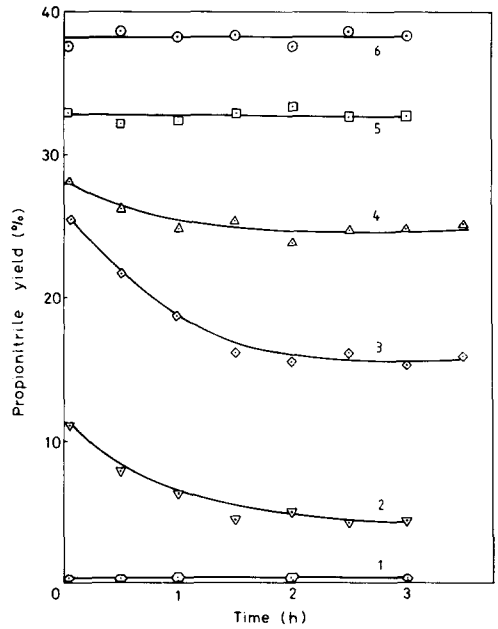

FIG. 4. Propionitrile yield as a function of reaction time under the standard reaction conditions for MoiSb samples. MoO_3 content (wt%): (1) 0.0 (pure α-Sb_2O_4), (2) 0.075, (3) 0.15, (4) 0.3, (5) 0.6, and (6) 1.2.

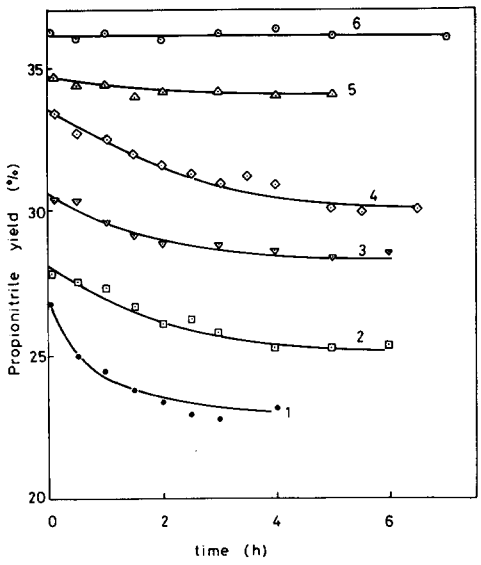

FIG. 5. Propionitrile yield as a function of reaction time under the standard reaction conditions for SbiMo samples. α-Sb_2O_4 content (wt%): (1) 0.0 (pure MoO_3), (2) 0.16, (3) 0.32, (4) 0.64, (5) 1.28, (6) 2.56.

90%; the selectivity does not change with a further increase of MoO_3 from 0.6 to 1.2 wt%.

3.2.2. Activity of SbiMo samples (MoO_3 Impregnated by Sb)

The evolution of the propionitrile yield as a function of time is presented in Fig. 5. All the samples impregnated with Sb show a yield higher than that of SbiMo0.0% (pure MoO_3). The samples containing 0.16, 0.32, and 0.64 wt% of α-Sb_2O_4 are not stable; their yields decrease progressively during the reaction. The yields of the samples containing 1.28 and 2.56 wt% of α-Sb_2O_4 do not change with reaction time.

The propionitrile yield of the different samples stabilizes after 3 h of reaction. A marked increase of yield is observed when the α-Sb_2O_4 contents in the samples are increased.

The propionitrile selectivity remains practically the same during the reaction. It is always near 95%.

3.3. CHARACTERIZATION RESULTS

3.3.1. Mechanical Mixtures (Ms) Samples before Reaction

The ultrasound mixing of the oxides in *n*-pentane does not bring about any noticeable modification of the BET surface area. It remains $2 m^2 g^{-1}$ for Ms0.0, Ms0.5, and Ms1.0.

The surface areas of the mechanical mixture obtained by ultrasound mixing correspond exactly to those of the individual constituents (namely $2 m^2 \cdot g^{-1}$). No fragmentation or roughening of the surface takes place.

The XRD spectra of the pure MoO_3 and α-Sb_2O_4 obtained from the various preparations always show the lines characteristic of the orthorhombic phases. The patterns of the Ms mixtures are exactly the superposition of those corresponding to the pure oxides. Neither new peaks nor any shift of the position are observed. Dispersion of the oxides in *n*-pentane does not modify the phases. The 020, 040, and 060 lines of MoO_3 have higher intensities than the others.

The Ms mixtures were analyzed by ESR. No signal was observed at 25 or -196°C from 1000 to 5000 Gauss.

Figure 6 shows the micrograph of the Ms0.5 sample taken with SEM. The dimension of particles for both oxides is between 0.5 and 2 μm. No smaller microcrystallites were detected. The MoO_3 particles are in the form of a large plate. The particles (marked 1) of α-Sb_2O_4 are closely surrounded by several particles of MoO_3 (marked 2). Conversely, the MoO_3 platelets are always surrounded by several α-Sb_2O_4 particles.

Analytical electron microscopy of a great number of the α-Sb_2O_4 and MoO_3 particles shows no traces of mutual contamination, in spite of the close contact between phases.

XPS results for the Ms0.5 sample indicate that the oxidation states of Sb and Mo in Ms samples before reaction are always identical to those characteristic of α-Sb_2O_4 and MoO_3 (*2*).

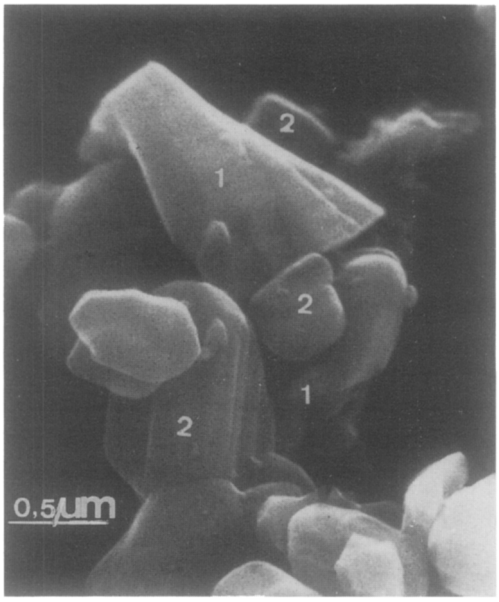

FIG. 6. SEM micrograph of Ms0.5 sample: (1) α-Sb_2O_4 particles, and (2) MoO_3 particles.

The relative analyzed concentration as a function of the atom ratio for Ms samples, is presented in Fig. 7. The intensity of Mo3*d* and that of Sb3$d_{3/2}$, measured by XPS, is proportional to the content of each element in the mixture. There is no measurable enrichment in either Mo or Sb in the outmost layers for the Ms samples.

The ISS intensities of Mo and Sb in the Ms0.5 sample as a function of the ion dose are presented in Fig. 8. After a modest initial rise, the Mo and Sb intensities do not change with the ions fluence. Table 2 gives the ISS surface composition results. For the Ms sample, the surface composition detected by ISS is practically the same as that of the bulk composition.

3.3.2. Mechanical Mixtures (Ms) Samples after Reaction

For the Ms samples used under the standard conditions, the post-reaction characterization by BET, XRD, SEM, AEM, XPS, ISS, and ESR gives exactly the same results as those obtained before the reaction (Figs. 6–8). On the other hand, no carbon deposit was detected for the Ms samples used in the presence of oxygen.

For the Ms samples used for 8 h in the *absence* of oxygen, the post-reaction characterization indicates some differences compared with the results for the fresh Ms samples:

- No carbon deposit was detected on Ms0.0. On the contrary, a large quantity of carbon deposit (2.81%) was detected on Ms1.0. The quantity detected on the Ms0.5 sample (1.24%) is less than that on Ms1.0, even (slightly but significantly) when calculated with respect to MoO_3 (C%/r) in the sample.
- The XPS spectra of the Ms0.5 used in the absence of oxygen indicate that both the Sb and Mo signals were slightly reduced, and changes in the binding energies indicated some reduction especially of Mo (*2*). The relative analyzed concentration of Sb3$d_{3/2}$ remained practically the same, whereas

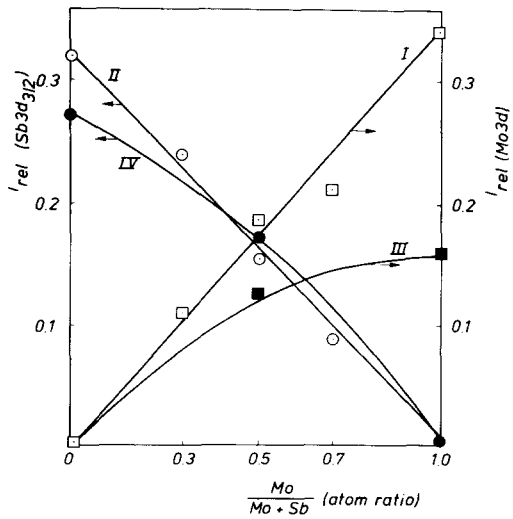

FIG. 7. XPS analysed concentrations of Mo and Sb in Ms samples as a function of composition *r*: Mo (□) and Sb (○) before reaction *and* after reaction under standard conditions; Mo (●) and Sb (■) after reaction in absence of oxygen.

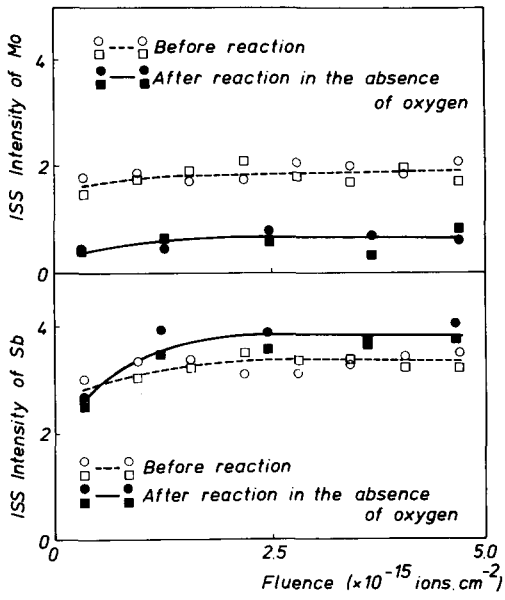

FIG. 8. ISS intensities of Mo and Sb in Ms0.5 sample as function of ion dose Symbols indicate reproducibility of measurements; ○ and □ before reaction (same values after standard reaction conditions); ● and ■ after reaction in the absence of oxygen.

that of Mo3*d* decreased when compared with the fresh samples (Fig. 7). Another observation with XPS is a marked increase of the carbon signal.

The ISS results concerning the Ms0.5 sample are presented in Fig. 8. Under standard conditions, the intensities of Mo and Sb are the same as those obtained in the fresh samples (white symbols). After the Ms0.5 sample has worked for 8 h in the absence of oxygen, the Mo intensity is much lower and the Sb intensity is slightly higher than those corresponding, respectively, to Mo and Sb in the fresh sample.

From the SEM micrographs it can be observed that the MoO_3 and α-Sb_2O_4 particles after working in the absence of oxygen were still composed of the pure oxide (AEM) and remained in good contact with each other.

3.3.3. Impregnated Samples (MoiSb and SbiMo) before Reaction

The surface areas of MoiSb and SbiMo have the value characteristic of the oxide playing the role of support (α-Sb_2O_4, 2.0 m^2 g^{-1}; MoO_3, 2.0 m^2 g^{-1}).

The XRD spectra give only the lines characteristic of the supports (α-Sb_2O_4 for MoiSb and MoO_3 for SbiMo).

Figure 9 presents the CTEM micrograph of the MoiSb1.2% sample. Microanalysis shows that the α-Sb_2O_4 particles, with dimensions of 0.5–2 μm, are pure: no Mo signal can be detected on those particles. The particles of MoO_3 are small, in the form of thin slices with a diameter of about 0.03–0.05 μm; they are well dispersed on the surface of the α-Sb_2O_4 particles and are also pure.

Figure 10 presents the CTEM micrograph of the SbiMo2.56% sample. Microanalysis shows that the α-Sb_2O_4 forms small uncontaminated particles in the shape of thin slices with a diameter of about 0.05–0.1 μm; the MoO_3 particles, with a diameter of 0.5–2 μm are pure (no Sb signal can be detected on them).

The XPS results are presented in Tables 3 and 4. The binding energy (BE) at 540.8 eV is that of Sb3$d_{3/2}$ electrons in α-Sb_2O_4 (*26, 35*) and those at 236.0 and 233.0 eV correspond to Mo3$d_{3/2}$ and Mo3$d_{5/2}$ electrons, respectively, in MoO_3 (*36–38*). The oxidation state of Sb and Mo in our samples is always identical to those characteristic of α-Sb_2O_4 and MoO_3.

The relative analyzed concentrations, deduced from XPS, are also given in Tables 3

TABLE 2

Mo and Sb Surface Composition Detected by ISS

Samples	Surface composition	
	MoO_3 (wt%)	Sb_2O_4 (wt%)
Ms0.3	31	69
Ms0.5	49	51
Ms0.7	71	29

Note. For each sample, the data are the average value of several measurements. Maximum relative experimental error is about 10%.

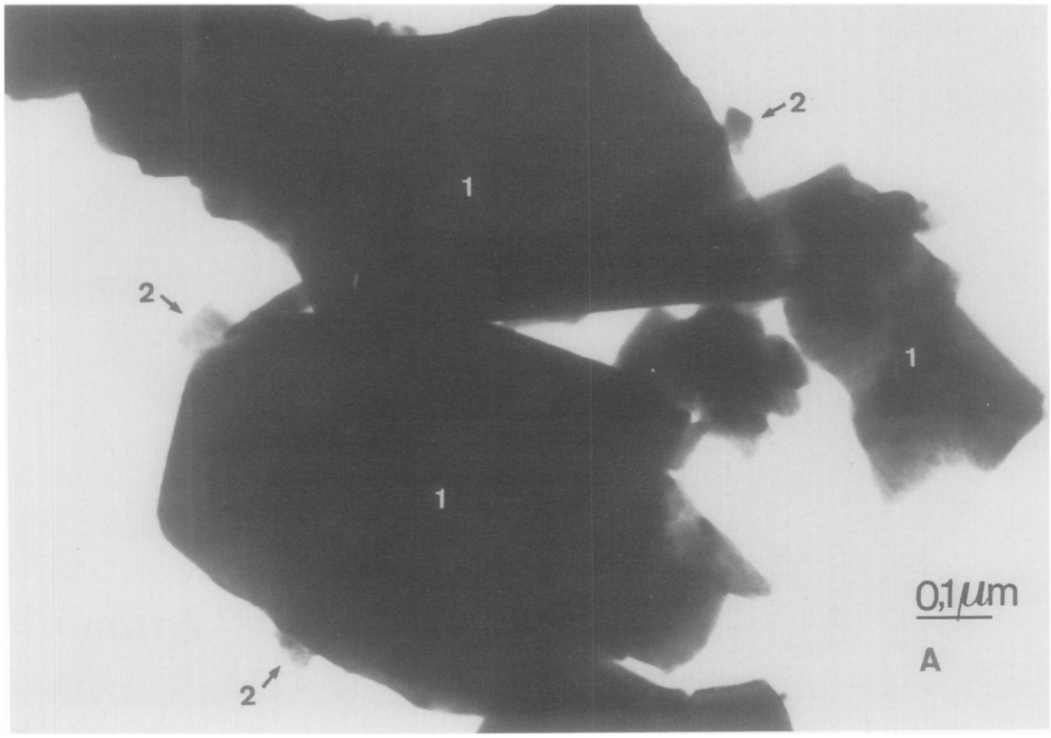

FIG. 9. CTEM micrograph of MoiSb1.2% sample: (1) α-Sb_2O_4 particles, and (2) MoO_3 particles.

and 4. The concentrations are compared with the values obtained from mechanical mixtures (Ms) containing the corresponding amounts of MoO_3 and α-Sb_2O_4. For the MoiSb samples, there is a strong increase in Mo3*d* intensity accompanied by a slight decrease in $Sb3d_{3/2}$ compared to the values of the mechanical mixtures. For SbiMo samples, the intensity of the Mo3*d* line is close to the values of the Ms samples while for the Sb phase, the $Sb3d_{3/2}$ intensities are higher than those in the mechanical mixtures.

The ISS intensities as a function of ion dose for the MoiSb1.2% sample are presented in Fig. 11. The Mo intensity decreases with the ion dose increasing from 0.9×10^{15} to 2.8×10^{15} ions cm^{-2}. On the contrary, the Sb intensity increases. When the ion dose reaches a value higher than 2.8×10^{15} ions cm^{-2}, both Mo and Sb intensities reach a plateau. The present results show that a partial contaminating layer of approximately one molecular thickness exists on fresh MoiSb 1.2% catalysts.

For the SbiMo2.56% sample (no figure presented here), the intensities of Mo and Sb remain practically unchanged with the ions fluences. No indication of partial contamining layer was detected.

Table 5 gives the ISS results. The surface composition of the MoiSb1.2% sample detected by ISS at the ion dose of 0.9×10^{15} ions cm^{-2} is 12% of MoO_3 (and 88% of α-Sb_2O_4). This MoO_3 content decreases to 7% for an ion dose of 4×10^{15} ions cm^{-2}. (The α-Sb_2O_4 increases to 93%).

The surface composition of the SbiMo2.56% sample does not change with the ions fluence. It always remains about 93% of MoO_3 with 7% of α-Sb_2O_4.

3.3.4. Impregnated Samples (MoiSb and SbiMo) after Reaction

(*a*) *MoiSb samples.* No carbon deposit was detected on these samples.

The BET surface area remains 2 $m^2 g^{-1}$, the same as that obtained for the fresh MoiSb samples. Even after catalytic work,

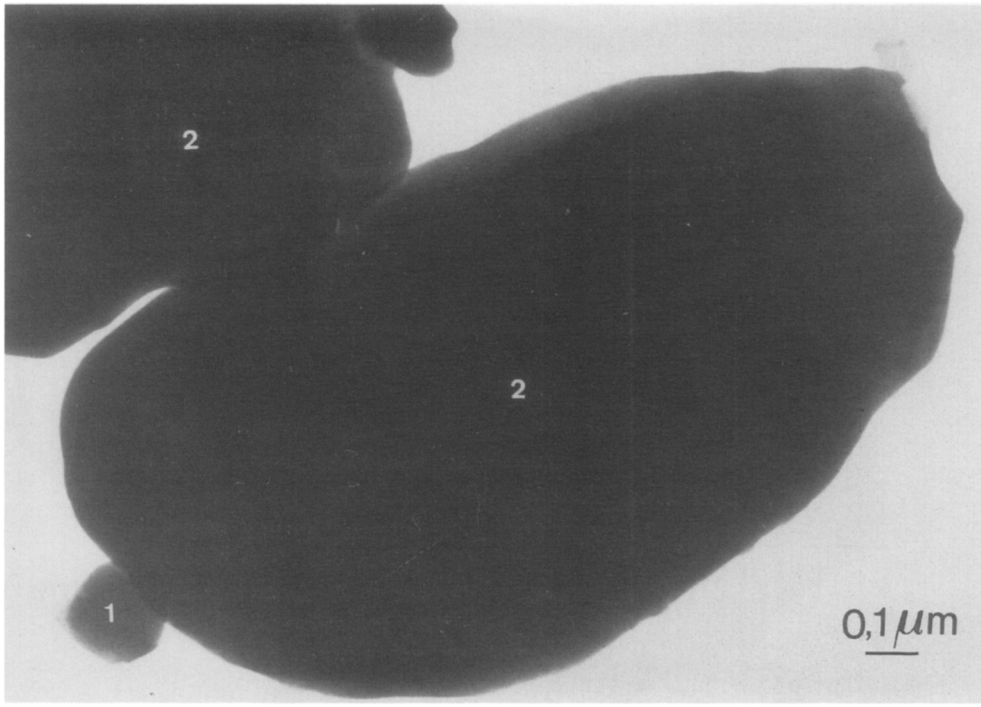

FIG. 10. CTEM micrograph of SbiMo2.56% sample (1) α-Sb_2O_4 particles, and (2) MoO_3 particles.

no fragmentation or formation of microcrystallites of the supporting oxide corresponding to a measurable increase of the surface area can be detected.

CTEM micrographs of the MoiSb1.2% sample show that, after reaction, the α-Sb_2O_4 particles do not change, but the small MoO_3 crystals (0.03–0.05 μm) become larger (0.1 μm). The X-ray microanalysis shows that the particles of MoO_3 and those of α-Sb_2O_4 are always pure.

XPS results are presented in Table 3.

TABLE 3

XPS Binding Energies and Relative Analysed Concentration of MoiSb Samples before and after Reaction. Ms are Mechanical Mixtures Containing the Corresponding Amount of MoO_3 and α-Sb_2O_4

	Before reaction		After reaction	
	0.15%MoO_3	1.20%MoO_3	0.15%MoO_3	1.20%MoO_3
Mo3$d_{5/2}$	233.0 eV	233.0 eV	233.1 eV	232.9 eV
Mo3$d_{3/2}$	236.0 eV	236.2 eV	236.0 eV	235.9 eV
Sb3$d_{3/2}$	540.4 eV	540.6 eV	540.3 eV	540.3 eV
		$I_{rel(Mo3d)}$		
MoiSb	0.037	0.092	0.022	0.084
Ms	0.0017	0.013		
		$I_{rel(Sb3d3/2)}$		
MoiSb	0.27	0.27	0.29	0.28
Ms	0.29	0.29		

TABLE 4

XPS Binding Energies and Relative Analysed Concentration of SbiMo Samples before and after Reaction. Ms are Mechanical Mixtures Containing the Corresponding Amounts of MoO_3 and α-Sb_2O_4

	Before reaction		After reaction	
	0.32%α-Sb_2O_4	2.56%α-Sb_2O_4	0.32%α-Sb_2O_4	2.56%α-Sb_2O_4
Mo3$d_{5/2}$	233.2 eV	233.4 eV	233.0 eV	233.2 eV
Mo3$d_{3/2}$	236.3 eV	236.4 eV	236.1 eV	236.1 eV
Sb3$d_{3/2}$	540.8 eV	540.9 eV	540.5 eV	540.6 eV
		$I_{rel(Mo3d)}$		
SbiMo	0.30	0.28	0.31	0.29
Ms	0.31	0.29		
		$I_{rel(Sb3d3/2)}$		
SbiMo	0.027	0.084	0.011	0.079
Ms	0.0037	0.032		

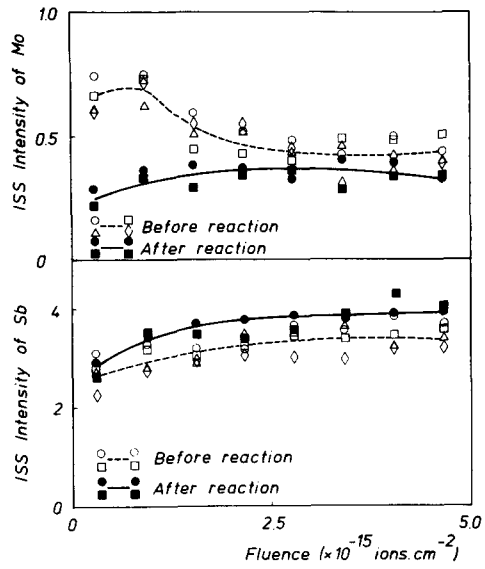

FIG. 11. ISS intensity of Sb and Mo in MoiSb1.2% as a function of ion dose. Symbols indicate reproducibility of measurements.

After reaction, the oxidation states of Sb and Mo remain the same as those characteristic of α-Sb_2O_4 (*26, 35*) and MoO_3 (*36–38*). The intensity corresponding to Mo3*d* after reaction, compared with that before reaction shows a decrease for MoiSb1.2% and a remarkable decrease for MoiSb0.15% is observed. The intensity corrsponding to $Sb3d_{3/2}$ for both samples increases slightly after reaction.

The ISS intensities of Mo and Sb as a function of ion dose for the MoiSb1.2% sample are presented in Fig. 11. After reaction, the Mo intensity does not change with the ion dose. Its value is very close to that for the fresh sample at an ion dose higher than 2.8×10^{15} ions cm^{-2}. The maximum of Mo intensity for the fresh sample at 0.9×10^{15} ions cm^{-2} has thus disappeared after reaction. A very slight increase of Sb intensity (if any) in the range of ion dose higher than 0.9×10^{15} ions cm^{-2} is observed when comparing the sample after the reaction with the fresh one.

(*b*) *SbiMo samples.* No carbon deposit was detected on these samples.

The BET surface area remains about 2 $m^2 g^{-1}$, similar to that obtained for fresh SbiMo samples. No fragmentation or formation of microcrystallites of the supporting oxide can be detected.

CTEM micrographs of the SbiMo2.56% sample show that, after reaction, the MoO_3 particles remain the same as those in the fresh sample, but the small α-Sb_2O_4 crystals become slightly larger. Before reaction, the thin slices of α-Sb_2O_4 have a diameter of about 0.05–0.10 μm. After reaction, this diameter increases to about 0.1–0.15 μm.

The X-ray microanalysis shows that the particles of MoO_3 and those of α-Sb_2O_4 are always pure.

XPS results are presented in Table 4. After reaction, the binding energies of $Sb3d_{3/2}$, $Mo3d_{5/2}$ and $Mo3d_{3/2}$ correspond to those characteristic of α-Sb_2O_4 (*26, 35*) and MoO_3 (*36–38*). A comparison of the intensity corresponding to Mo3d after reaction with that before reaction shows only a very modest increase. For the intensity corresponding to $Sb3d_{3/2}$, a marked decrease for SbiMo0.32% and a very slight decrease for SbiMo2.56% are detected.

ISS intensities of Mo and Sb as a function of ion dose for the SbiMo2.56% sample show that, in the whole range of the ion dose, a decrease of Sb intensity accompanied by a very slight increase of Mo intensity (if any) is observed when comparing the sample after reaction with the fresh one.

TABLE 5

Mo and Sb ISS Surface Composition[a]

Samples	Mo at maximum[b]		In deep layers[c]	
	MoO_3(wt%)	Sb_2O_4(wt%)	MoO_3(wt%)	Sb_2O_4(wt%)
MoiSb1.2%	12	88	7	93
SbiMo2.56%			93	7

[a] For each sample, the data are the average value of several measurements. Maximum relative experimental error is about 10%.

[b] For MoiSb, at the ion dose 0.9×10^{15} ions cm^{-2} (Fig. 5). For SbiMo, no maximum was observed.

[c] Surface composition detected at the ion dose 4×10^{15} ions cm^{-2} where the Mo and Sb intensities are constant.

3.3.5 Solid State Synthesis (Ss) and Coprecipitation by Evaporation of Aqueous Solution (Cs)

All preparations give the same crystallographic characteristics of α-Sb_2O_4 and MoO_3 phases. No new peak nor shift of position is observed by X-ray diffraction analysis. No signal was observed by ESR at 25 or -196°C from 1000 to 5000 Gauss.

4. DISCUSSION

For a catalyst constituted of two or several phases, several possible modifications in composition or structure during preparation may be considered, e.g., formation of a solid solution or a new compound, contamination of one phase by another, or partial or complete formation of a monolayer of one phase on the surface of the other (or other types of structure in epitaxial contact with that surface). To arrive at a correct understanding of the nature and structure of the catalyst, an analysis with a combination of characterization techniques is necessary. As the relative average composition of the surface detected by the physico-chemical characterization methods might be influenced by the morphology of particles and the presence of aggregates, we must necessarily discuss these last effects before concluding of the formation of a contamination or a monolayer. We shall examine all these possibilities bearing in mind other results to be found in the literature as well as the results of our characterization experiments.

4.1. Possibility of Formation of Solid Solution or Mixed Phase

The data found in the literature dealing with the formation of ternary Mo–Sb–O compounds are listed in Table 6.

For the MoO_3 + α-Sb_2O_4 system, the formation of ternary Mo–Sb–O compounds only takes place in very severe (and, apparently, relatively reducing) conditions and, when formed, these compounds decompose spontaneously into MoO_3 and Sb_2O_4 in the range of temperatures investigated in this paper.

The methods usually used to detect the Mo–Sb–O compounds are XRD and especially ESR spectroscopy because of its high sensitivity, taking into account the nature of Mo, one of the elements involved in the mixture. In fact, the data in the literature indicate that when Mo–Sb–O compounds are formed, an ESR signal situated around a g value of 1.92 can always be observed (*41*).

The Ss and Cs samples were prepared in experimental conditions designed to maximize the formation of a mixed oxide or a solid solution. Nevertheless, the X-ray diffraction spectra of these samples present only the lines characteristic of pure MoO_3 and/or α-Sb_2O_4 oxides. The examination by ESR in high sensitivity conditions did not permit to detect any signal. This rules out the formation of Mo–Sb–O compounds or solid solution. Indeed, our samples were always calcined in air at a temperature equal or lower than 600°C. These conditions do not correspond to those where the formation of a Mo–Sb–O compound or a solid solution is possible (Table 6). In addition all the other samples (mechanical mixtures or impregnation) present only the XRD lines characteristics of pure MoO_3 and α-Sb_2O_4. No new lines are observed. No signal could be detected by ESR.

4.2. Sample Morphology and Aggregation

(*a*) *Mechanical mixtures (Ms).* The SEM micrographs show that the majority of MoO_3 particles in Ms samples have the form of large plates which expose predominantly the 010 face (Fig. 6). This is confirmed by XRD results: the reflections of the planes parallel to plate faces (020, 040, 060) is more intense that that of other faces. The Ms samples are composed of MoO_3 and α-Sb_2O_4 particles of similar size. The two phases are well interdispersed during the preparation of catalysts and the particles of different oxides are in good mutual contact. No auto-

TABLE 6

Mo–Sb–O Compounds and Solid Solution

Attempt to produce the following Mo–Sb–O compounds	Preparation conditions	Results, additional remarks or solid solution	References
$[Sb_2(MoO_4)_3]$	MoO_3 + Sb_2O_3 in air 700–1100°C, 264 h	No mixed compound obtained	(*22, 23*)
Sb_2MoO_6	MoO_3 + Sb_2O_3 600 Torr Ar, 500°C, 48 h	Decomposition: $Sb_2MoO_6 \xrightarrow[400°C]{air} MoO_3 + \alpha\text{-}Sb_2O_4$	(*24*)
$[Sb_2(MoO_4)_3]$	Same as Sb_2MoO_6 above	Same as Sb_2MoO_6 above	(*24*)
$Sb_{0.2}MoO_{3.1}$	Reduction of Sb_2MoO_6 + MoO_3	$Sb_{0.2}MoO_{3.1} \xrightarrow[350°C]{air} MoO_3 + Sb_2O_4$	(*25*)
$Sb_{0.4}MoO_{3.1}$	Same as $Sb_{0.2}MoO_{3.1}$ above	$Sb_{0.4}MoO_{3.1} \xrightarrow[300°C]{air} MoO_3 + Sb_2O_4$	(*25*)
1.5% Mo in β-Sb_2O_4	MoO_3 + α-Sb_2O_4 in evacuated tube, 850°C, 80 h	Dissolution of Mo accompanied always by transition of α-Sb_2O_4 to β-Sb_2O_4	(*39, 40*)

aggregation of either MoO_3 or α-Sb_2O_4 is observed.

(*b*) *Impregnated samples.* The morphology of the impregnated samples is characterized by the presence of very small crystallites of the impregnated phase deposited on the much larger crystals of the other oxide acting as support. No aggregation is observed for either the MoiSb samples or the SbiMo samples. The small crystallites of the supported phase, which are about two orders of magnitude smaller than those of the support, are well dispersed on the surface of the latter (Figs. 9 and 10).

4.3. Possibility of Contamination or Monolayer Formation during Preparation

In principle, accidental contamination by elements different from Mo or Sb could take place during preparation, if trace impurities were present in the reagents. We checked carefully that this possibility should be excluded. All the initial materials used for catalyst preparation were analytically pure-grade. The use of a saturated hydrocarbon (*n*-pentane) for mechanically mixing the powders minimized the possibilities of dissolving salts which could get deposited on MoO_3 or Sb_2O_4. Careful examination of the XPS spectra (and AEM peaks) did not indicate the presence of any element other than Mo, Sb, O, and C in detectable quantities. We must consider that, with the precision of the various analytical methods used, our samples contain only pure molybdenum and antimony oxides.

Another problem corresponds to the possibility of mutual contamination of molybdenum oxide and antimony oxide. This problem will be examined in what follows.

For a sample containing two phases in simple physical contact, if the particles of *A* and *B* have a similar size and are well dispersed, the surface composition measured by XPS and ISS should be directly proportional to the bulk composition of the samples. If there exists an aggregation or even an agglomeration of the particles of one phase, its intensity should be lower.

In the case of a sample composed of two phases of different sizes, for example, with small *A* particles and large *B* particles, if the *B* particles are surrounded by *A*, the

intensity of *A* detected by XPS and ISS should be greater than that of *B* and, consequently, an apparent surface enrichment of *A* should be observed.

For a sample where *B* is contaminated by *A* or a partial or total monolayer of *A* (or any other surface species containing *A*) forms on the surface of *B*, AEM and XPS could detect a surface enrichment of phase *A* (but it would be difficult to distinguish cases where either contamination by *A* or *A* monolayer formation would occur, from cases where very small crystallites of *A* would be deposited on the surface of *B*, because of the low resolution of AEM and the relatively deep sampling depth of XPS). To investigate surface composition, ISS is more sensitive than AEM and XPS. If a surface contamination or monolayer of element *A* exists, the ISS intensity of *A* should diminish during the sputtering, due to erosion of the surface by the Ne ions of 2 keV, to a constant value which reflects the average composition in bulk.

With this information in mind, we shall discuss the results obtained by AEM, XPS, and ISS.

(*a*) *Mechanical mixtures* (*Ms*). AEM shows that the Ms samples are composed of pure MoO_3 and pure α-Sb_2O_4 particles. No surface enrichment of either MoO_3 or α-Sb_2O_4 can be detected by XPS and ISS. More specifically, the ISS intensity of Mo and Sb in Ms samples (except for the initial very modest rise) does not change with the ions fluence during the sputtering; the composition at the surface is the same as that in the bulk. The initial rise is common in ISS measurements. It is due to the desorption under the impact of ions of lower mass impurities, such as oxygen or water adsorbed on the surface (*42*). As a conclusion, no indication of a partial contaminating layer was observed in our samples.

We thus have to conclude that the Ms samples are composed of pure, uncontaminated MoO_3 and α-Sb_2O_4 oxides, in physical contact when mixed together.

(*b*) *Impregnated samples*. CTEM, AEM, XPS, and ISS indicate that a relatively important masking of the surface of Sb_2O_4 is brought about by MoO_3 during the preparation of MoiSb samples. MoO_3 probably forms "patches", monolayers or multilayers and microcrystallites of MoO_3. The situation for SbiMo samples is completely different: no monolayer or contamination of α-Sb_2O_4 is detected by ISS or any other technique.

4.4. Evolution of the Architecture of Catalysts during the Reaction

(*a*) *Mechanical Mixtures*

An important fact is that the uncontaminated oxides forming the mechanical mixtures are not modified during the catalytic reaction, except in the case where the oxygen concentration is low. No modification of the samples can be detected by either ISS, XPS, or AEM. We note the results of the very sensitive surface techniques on ISS. The ISS intensities for fresh and used samples are exactly the same (Fig. 8).

(*b*) *Impregnated Samples*

(*b1*) *MoiSb samples*. ISS indicates that the partial coverage of Sb_2O_4 by MoO_3 is destroyed during reaction (disappearance of the maximum of Mo intensity and the increase of Sb intensity). This implies that there is a detachment of the contaminating layer and a transformation of the microcrystallites of MoO_3 into crystals of larger size, as shown by CTEM. XPS confirms this observation. The decrease of the XPS Mo intensity for a sample containing a low MoO_3 content (MoiSb0.15%) is more pronounced than that with higher MoO_3 contents (MoiSb1.2%).

The results show that contamination (possibly patches of monolayer or multilayer) and microcrystallites of MoO_3 are not stable under the reaction conditions. They tend to form MoO_3 crystals of a larger size.

(*b2*) *SbiMo samples*. No monolayer or contamination of α-Sb_2O_4 is detected by ISS for any SbiMo sample after reaction. CTEM

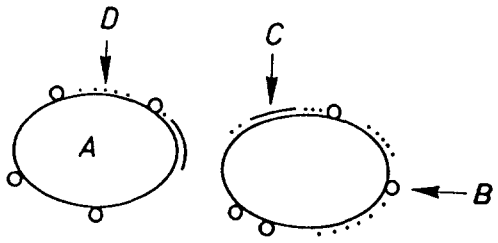

FIG. 12. MoiSb samples before reaction: (A) α-Sb_2O_4 particles, (B) MoO_3 particles, (C) Monolayer of MoO_3, and (D) Microcrystallites of MoO_3.

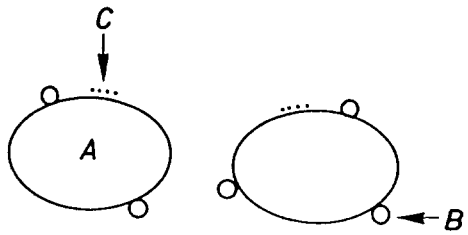

FIG. 13. MoiSb sample after reaction: (A) α-Sb_2O_4 particles, (B) MoO_3 particles, and (C) Microcrystallites of MoO_3.

shows that the small α-Sb_2O_4 crystals become larger after reaction. Indeed, XPS and ISS also detect a decrease of Sb intensity after reaction. This shows that the small crystals or microcrystallites of α-Sb_2O_4 are not stable and that they grow to crystals of a larger size during the reaction. This decreases the coverage of α-Sb_2O_4 on the surface.

These characterization results demonstrate in a conclusive way that there does not exist any tendency to spontaneous contamination or monolayer formation under the reaction conditions. On the contrary, if one creates a partial contamination or monolayer during the catalyst preparation, it disappears during the reaction. There is thus a conspicuous tendency of the associated oxides to segregate to two phases. This corresponds to a strong contrast compared to other two-phase systems containing MoO_3 in which there is a tendency of spontaneous contamination of the support of MoO_3 (*43*) (Examples of these systems are MoO_3 + Al_2O_3, MoO_3 + TiO_2, MoO_3 + SnO_2, and MoO_3 + MgO, but not MoO_3 + SiO_2, in which some tendency of MoO_3 to detach from SiO_2 is observed).

The evolution of the architecture of the impregnated catalysts is presented schematically in Figs. 12, 13, 14 and 15.

4.5 Carbon Deposition

A carbon deposit was detected on Ms1.0 (MoO_3) but not on Ms0.0 (α-Sb_2O_4), after the samples had worked for 8 h in the absence of oxygen. The Sb intensity increased slightly (XPS and ISS). The marked decrease of the intensity corresponded only to the signal of Mo (XPS and ISS). This is due to coke formation brought about by some side reaction. In the mixture, carbon is preferentially deposited on the surface of MoO_3. No carbon deposit was detected in MoiSb or SbiMo samples.

4.6. Correlation of Catalytic Activity with Architecture and Physico-Chemical Properties of Catalysts

It should be emphasized that the pure α-Sb_2O_4 and pure MoO_3 samples in each series of samples (Ms, SbiMo, MoiSb) were subjected to the same series of treatments as the other samples. Accurate comparisons may thus be done.

There is a synergy between uncontaminated α-Sb_2O_4 and uncontaminated MoO_3 in the Ms mixtures. The magnitude of the synergy depends on the surface area developed by each phase, or more precisely, on a proper balance between the extends of both surface areas (Fig. 1). Presumably, it also should depend on the intimacy of the contacts of the two phases.

The physico-chemical characterization of the catalysts excludes the following possible explanations for the synergy: (i) the formation of a mixed oxide or solid solution, (ii) the contamination of one oxide by the elements of the other, and (iii) any change in surface area of MoO_3 (the specific surface

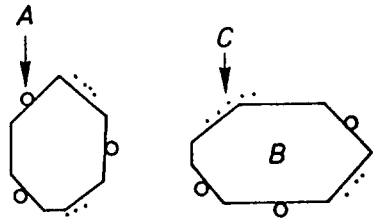

FIG. 14. SbiMo sample before reaction: (A) α-Sb_2O_4 particles, (B) MoO_3 particles, and (C) Microcrystallites of α-Sb_2O_4.

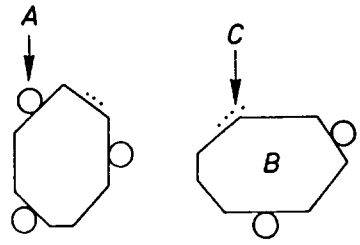

FIG. 15. SbiMo sample after reaction: (A) α-Sb_2O_4 particles, (B) MoO_3 particles, and (C) Microcrystallites of α-Sb_2O_4.

area of the mixed samples remains equal to $2m^2\ g^{-1}$ whichever the composition, and no MoO_3 microcrystallites, as could have been formed by hypothetical mechanical damage to the initial MoO_3 crystals, could be detected by CTEM).

We note that the preparation methods used in order to maximize the mixed oxide or a solid solution formation (S_s and C_s samples) show in an unquestionable way that no new oxide phase, different from α-Sb_2O_4 and MoO_3, was formed.

Although the data concerning the noncontamination are convincing and the tendency of the Mo and Sb oxide species to detach from each other is obviously very strong, it may be useful to develop another argument for proving that a contamination, if it existed (at an undetectable level), would not be compatible with our results.

If we accepted the assumption that the synergy were due to partial contamination, the active phase would be α-Sb_2O_4 contaminated by MoO_3. The synergistic effect would become important as soon as a sufficient quantity of MoO_3 would be present to cover a substantial fraction of the α-Sb_2O_4 surface. Due to the high mobility of MoO_3 (volatility, surface migration) often mentioned in literature, the contamination would not depend critically on the perfect intermixing of the MoO_3 particles with those of the other oxide. It would be sufficient that an amount of MoO_3 comparable to that necessary to cover the surface of α-Sb_2O_4 be present in the mechanical mixture for observing the maximum synergetic effect. This can be calculated. Considering that one MoO_3 molecule in a monolayer structure covers 0.17 nm^2 (*29*), the MoO_3 contents required to form a monolayer on the α-Sb_2O_4 samples of different surface areas were calculated. They are given in Table 7. If the assumption mentioned above were correct, we should observe the maxima of synergy around the calculated values of mass ratio r indicated in the table. The actual position of the maxima are situated at mass ratios r very different from those values. This shows that the hypothesis of contamination is totally inconsistent with our results. Even assuming that MoO_3 is very mobile, it does not adhere to α-Sb_2O_4 (let us remark that in order to remain undetected, this contamination should actually be much lower than that corresponding to a monolayer, with the implication that the maximum of activity should occur at still lower r values).

Under the standard reaction conditions, the activity of the following samples decreases as a function of the reaction time:

1. MoiSb samples containing less than 0.6 wt% MoO_3 (Fig. 4);

2. SbiMo samples containing less than 1.28 wt% α-Sb_2O_4 (Fig. 5).

In general, the decrease in activity may be due either to a decrease of a beneficial contamination, or, if no such beneficial contamination exists, to a change of the optimum balance between the two surface areas of the two oxides, account taken of their

TABLE 7

Calculated Quantities of MoO_3 to Form a Monolayer on the α-Sb_2O_4 of Different Surface Areas and Actual Position of Maximum Synergy Obtained by Experiments for the Corresponding Two-phase Catalysts

Samples	Surface area ($m^2\ g^{-1}$)	MoO_3 content for a monolayer (Wt%)	Calculated value of r for complete monolayer formation	Actual position of the maximum of synergy (r) from Fig. 1
Ms	0.4	0.056	0.0006	0.25
Ms	2.0	0.280	0.0028	0.5
Ms	5.2	0.728	0.0072	0.75

contacts (number, quality), in the context of a remote control type of cooperation (which will be discussed in Section 4.7).

The results of the MoiSb samples give other important information. As calculated theoretically, 0.28 wt% of MoO_3 is sufficient to form a complete monolayer on the surface of α-Sb_2O_4 ($2\ m^2\ g^{-1}$). The activity increases with the MoO_3 content even when the content is higher than 0.3 wt% (Fig. 4). Moreover, as shown by ISS, the initial contamination of the fresh MoiSb1.2% sample disappears during the catalytic reaction, but the activity does not change with this disappearance of contamination and the synergetic effect still exists. This indicates that there exist important effects for the synergy other than contamination.

In a previous work (*4*) we had used a method different from impregnation by molybdenum oxalate for producing a partial contamination of α-Sb_2O_4 by Mo. The catalyst was prepared by impregnation of α-Sb_2O_4 with a solution containing the required quantity of $(NH_4)_6Mo_7O_2 \cdot 4H_2O$. The slurry was evaporated. The resulting solid was dried at 393 K for 15 h and then calcined at 703 K for 8 h in air.

We also found that this contaminating deposit of MoO_3 got detached from α-Sb_2O_4. The synergistic cooperation between α-Sb_2O_4 and MoO_3 still manifested itself. It became more important after the detachment of MoO_3 had proceeded.

Thus, we have no indication that a monolayer or a contaminating surface species, if it exists, is active and selective for the reaction. Rather, data show that separate MoO_3 particles are essential for activity.

In conclusion, we do not exclude the possibility that there still remains a minute contamination or a very small fraction of monolayer which cannot be detected by the physico-chemical characterization techniques, but there certainly exists another effect that is much more important for the catalytic synergy.

4.7. Remote Control Effect in the MoO_3 + α-Sb_2O_4 System

The above results lead us to conclude that there exists a cooperation between the MoO_3 and α-Sb_2O_4. Our explanation is that a remote control effect (*1–4, 44–46*), as mentioned in the introduction, does play an important role for the catalytic synergy.

In the case of the MoO_3 + α-Sb_2O_4 system, our results show that MoO_3 possesses a moderate activity in propionitrile formation and α-Sb_2O_4 alone is inert. MoO_3 carries the sites that are active in selective dehydration. When MoO_3 and α-Sb_2O_4 particles are mixed together, a conspicuous increase in the yield of propionitrile occurs: α-Sb_2O_4 increases the activity of MoO_3, presumably by increasing the number of sites active during the catalytic work. In the context of the remote control mechanism, the role of the controlling phase (α-Sb_2O_4, producing spillover oxygen) and that of the controlled

phase (MoO_3, giving catalytic sites for dehydration) can be clearly distinguished.

If there exists a control effect between two phases, the following aspects must be contemplated:

—The first concerns the role of oxygen. The basic aspect of the remote control mechanism is the existence of mobile oxygen species. The magnitude of the synergetic effect must be influenced by oxygen in the gas phase because the amount of spillover species produced must be dependent on oxygen pressure. Significant effects would be observed when the oxygen pressure is changed or when oxygen is absent.

—The second aspect concerns the contact between the two phases. If a control effect of one phase on the surface of the other solid occurs, it would be influenced by the following parameters:

1. The ratio of the surface areas developed by the two phases;
2. The number and quality of the contacts between the two phases.

Indeed, these parameters determine the average amount of spillover oxygen flowing on MoO_3 per unit surface area of MoO_3.

We shall examine the two aspects mentioned above in the following sections.

4.7.1. The Role of Oxygen

Figure 3 shows the influence of the oxygen pressure. The yield of propionitrile of the Ms0.5 samples increases more rapidly with oxygen pressure than that of the Ms1.0 (MoO_3) sample in the low value range ($P_{O_2} \leq 6$ Torr). This implies that α-Sb_2O_4 can produce the surface oxygen necessary for MoO_3 to be active in propionitrile formation, more efficiently than MoO_3 alone can. It is very interesting to note that the yield of the Ms0.5 sample does not change with a further increase of oxygen pressure beyond 6 Torr (from 6 to 45 Torr). This can be explained by the existence of a saturation phenomenon, i.e., 6 Torr of oxygen pressure suffices to produce enough spillover oxygen to maintain catalytic activity. But for Ms1.0, a much higher P_{O_2} is necessary to attain the activity plateau.

These results show more quantitatively the effect mentioned in our earlier publication, namely that MoO_3, in transient experiments, behaves differently from a MoO_3 + Sb_2O_4 mixture: we had shown in particular that the MoO_3 + Sb_2O_4 mixture very rapidly regains activity and selectivity when, after interruption of the O_2 supply, the latter is reestablished (*2*).

Another important remark is that, in the catalytic test, the amount of each sample used as catalyst was always 130 mg. An Ms0.5 sample thus contains 65 mg of MoO_3 and 65 mg of α-Sb_2O_4 (which is not active on its own). These 65 mg of MoO_3 bring about the transformation of more formamide molecules than 130 mg of pure MoO_3 (Fig. 2). This indicates that not only can spillover oxygen maintain catalytic activity, but it also can create new active sites for the reaction.

The originality of the two-phase catalysts containing MoO_3 is that they work efficiently in the dehydration of N-ethyl formamide only in the presence of dioxygen, in spite of the fact that O_2 does not participate in the stoichiometric reaction.

If the O_2 is suppressed from the feed, the propionitrile selectivity and the reaction conversion both decrease (Table 1). This implies that (i) the active sites are partly altered (decrease of selectivity), i.e., there is a change in the nature of the sites and (ii) they are partly inhibited (decrease of conversion), i.e., there is a disappearance of the sites. In that context, the deactivation observed in the absence of oxygen would be explained by the impossibility of spontaneous regeneration of active sites after an accidental destruction, alteration, or fouling. The decrease of the propionitrile selectivity (Table 1) is probably due to the superficial reduction of molybdenum, as indicated by the XPS measurements (*2*). The presence of carbon on the surface, resulting in the decrease of the number of accessible molybdenum atoms (Figs. 7 and 8) and conse-

quently the decrease in conversion (Table 1) after 8 h of time-on-stream in the absence of oxygen for Ms0.5 and Ms1.0 samples, strongly suggests that carbon (coke) is responsible for inhibition (fouling).

Results that we have presented previously support this view and explain them in some detail (*4*). We showed that MoO_3 was slightly reduced during reaction. The propionitrile *selectivity* decreased when the reduction degree increased. Coke got deposited in these conditions. It deposited selectively on the surface of MoO_3 (not on α-Sb_2O_4), and the *activity* decreased when the amount of carbon deposited increased.

Another important observation was that the reduction degree of MoO_3 and the amount of carbon deposited on MoO_3 decreased with the increase of α-Sb_2O_4 content in the mixture. The conclusion was that spillover oxygen produced by α-Sb_2O_4 acted by reoxidizing the reduced sites and cleaning the MoO_3 surface from coke during the catalytic reaction.

In normal operation in the presence of oxygen, molybdenum retains the correct oxidation state, maintaining the selectivity at about 95%. If we admit that, under the same conditions, small amounts of coke are continuously formed on the surface, although at a slower rate than when oxygen is absent, one could imagine that oxygen also continuously cleans that coke off the surface and the spillover oxygen can do this in a more efficient way. Indeed, a slight deactivation for Ms1.0 has been observed in the course of the reaction, but not for Ms0.5 (Fig. 2).

Although it does not correspond to any data in literature, a special hypothesis should be examined, namely that the small crystallites of α-Sb_2O_4 present on the surface of MoO_3 would prevent, by mere steric hindrance, the formation of large carbonaceous polymeric deposits. This hypothesis can be excluded by the experimental evidence presented in the second paper of this series. There, the carbon deposits were first deposited on the pure MoO_3 and then this carbon contaminated MoO_3 was mechanically mixed with α-Sb_2O_4. In that case, although the α-Sb_2O_4 was mixed after the deposition of carbon on the MoO_3 surface, the same phenomenon as reported here were observed. The removal of the deposit coke was also accelerated by the presence of α-Sb_2O_4 in the mixture.

In conclusion, our results show that spillover oxygen acts in two ways. It certainly acts against the formation of nonselective catalytic sites. Our results also strongly suggest that, in addition, it cleans the coke off the surface.

The decrease of selectivity with the increase of MoO_3 contents in MoiSb samples can be easily explained by considering the conclusion mentioned above. In fact, with the increase of MoO_3 content, the MoO_3 crystallites become larger. Thus, the spillover oxygen, emitted by α-Sb_2O_4, less efficiently reaches all the catalytic centers located on the MoO_3 particles and, consequently, less effectively controls their selectivity. For the MoiSb0.075% sample, the very small crystallites of MoO_3 are well dispersed on the surface of α-Sb_2O_4. The spillover oxygen can easily attain the whole surface of MoO_3 and protect it from reduction. This results in a practically 100% selectivity. For a MoiSb1.2% sample, the spillover oxygen must migrate a longer distance to attain the whole surface of the larger crystallites of MoO_3. This gives rise to a slightly lower selectivity (90%).

4.7.2. Surface Areas and Contact between the Two Phases

The remote control implies the formation of a spillover species, its transfer to another phase, and reaction on (with) that second phase. In a general way, the effect of spillover oxygen will be influenced by the relative surface areas of the phases, which determines the amount of spillover species potentially available per unit surface area of MoO_3. But these spillover species may actually reach the surface of MoO_3 more or less easily according to the number and intimacy of contacts between α-Sb_2O_4 and MoO_3.

The contacts thus determine the amount of spillover oxygen which can react with the surface of MoO_3 and/or the carbon deposited on it.

The displacement of the maxima of synergy for Ms samples (Fig. 1) constitutes an evidence that the ratio of surface areas developed by the two phases, rather than the bulk composition, is at stake in the synergy. When this ratio is near one, in other words when the total surface area developed by one phase is the same as that developed by the other phase in the mixture, the catalytic synergy attains the maximum. It should be emphasised that, in principle, this value of approximately one could be different for two-phase catalysts different from those used in the present study, as it depends on the respective rates of formation of O_{so} on the oxide dissociating O_2 to spillover species and the reaction of the latter on the potentially active phase.

For MoiSb (or SbiMo) samples, the impregnation of α-Sb_2O_4 (or MoO_3) with a small amount of Mo (or Sb) ions improves considerably the catalytic properties of the two-phase catalyst. It is remarkable, in this respect, that the yield of MoiSb1.2% or SbiMo2.56% is comparable to that of mechanical mixtures Ms0.5. For MoO_3 impregnated by Sb (SbiMo), the main favorable factor is certainly the fact that MoO_3 benefits from many more contacts with α-Sb_2O_4, present in the form of many small crystallites "decorating" MoO_3. For MoiSb, where small MoO_3 crystallites "decorate" α-Sb_2O_4, the comparison with the Ms series is difficult. MoO_3 is much more dispersed (but the low surface area values and the corresponding low relative accuracy of the measurements do not allow to evaluate the corresponding surface area). All crystallites are in contact with α-Sb_2O_4 and their small size makes that all points of their surface can be reached by spillover species. These two very favorable factors overcompensate the lower overall surface area developed by the MoO_3 crystallites, and give the MoiSb a high activity. For both types of impregnated samples, this illustrates the advantages of the impregnation method (*27, 28, 30*).

The activity of the MoiSb (SbiMo) samples increases when the Mo (or Sb) content increases (Figs. 4 and 5). This agrees with our hypothesis. In fact, the increase of the Mo (or Sb) content results in that the system approaches the adequate balance of the surface areas developed by both phases, and there is an increase of the number of contacts between them, consequently bringing about an increase of the yield.

Another observation is the decrease of yield during the first 2 to 4 h of work. This can be easily explained. For the MoiSb (or SbiMo) samples, a minimum content of Mo (or Sb) is necessary to form the stable particles of the oxide of the added element. If the content is lower than that minimum, the particles are too small, unstable, and they tend to aggregate in order to form stable particles, resulting in the decrease of contact number and of surface area developed by Mo (or Sb). This minimum is about 0.6 wt% MoO_3 for MoiSb and 1.28 wt% α-Sb_2O_4 for SbiMo samples respectively. Above that minimum, the yield is stable (Figs. 4 and 5).

With the intervention of a remote control effect, as shown schematically in Fig. 16, a sufficiently high content of α-Sb_2O_4 can produce enough spillover oxygen and, if there are sufficient points of contact with MoO_3, this oxygen can regenerate the deactivated sites by reoxidizing the reduced sites and cleaning the MoO_3 surface by continuously removing coke during the reaction. This process is more efficient than the direct intervention of gaseous oxygen O_2 reacting directly with the surface of MoO_3.

As a continuation of this study, more direct experimental evidence for the remote control mechanism, such as identification of the nature of the active site, and evidence of spillover oxygen and of its migration from its site of generation to the site of activity, will be the object of the second paper of this series.

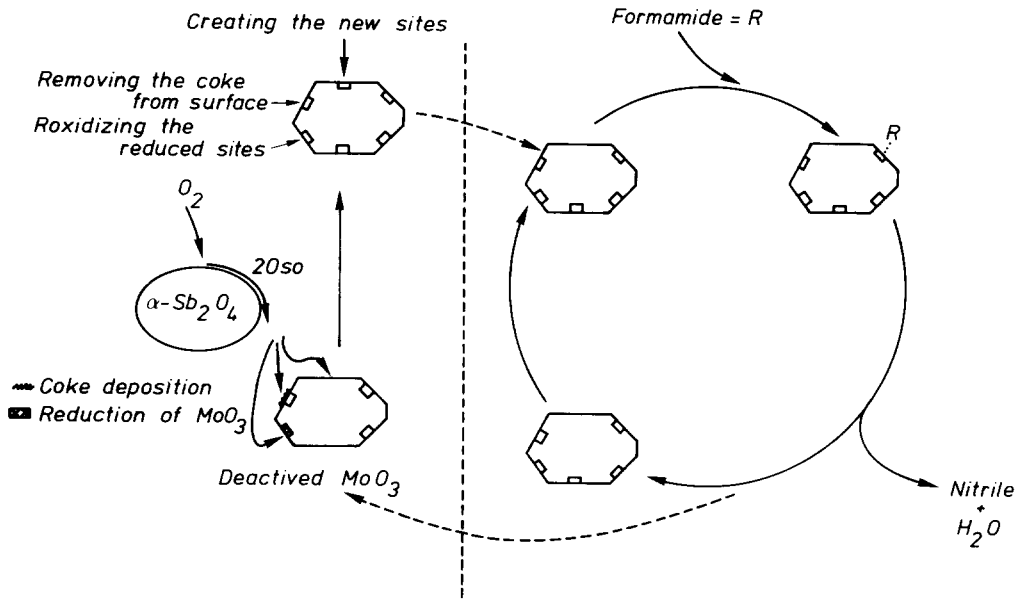

FIG. 16. Representation of the remote control mechanism.

5. CONCLUSIONS

The detailed physico-chemical characterization of our α-Sb_2O_4-MoO_3 samples prepared by different methods excludes the formation of any Mo–Sb–O compound or solid solution and any sort of detectable mutual contamination. Rather, when one of the oxides is depostied on the other by impregnation, it exhibits a strong tendency to detach from its surface.

A strong catalytic synergy is detected in mechanical mixtures of uncontaminated MoO_3 and α-Sb_2O_4. With impregnated catalysts, the synergy persists after the segregation of the two phases. It is thus impossible to attribute the synergy to the contamination or monolayer formation of one phase on the other. The origin of the synergy is a specific cooperation between pure MoO_3 and α-Sb_2O_4 phases, via a remote control mechanism. MoO_3, as a controlled phase, carries the active sites for the reaction. α-Sb_2O_4, as a controlling phase, activates (dissociates) gaseous oxygen into a mobile oxygen species (spillover oxygen). This spillover oxygen, as the controlling species, can migrate from α-Sb_2O_4 onto the surface of MoO_3 where it creates new active sites and/or regenerates the deactivated sites by reoxidizing the reduced MoO_3 and cleaning the coke deposits off the surface.

6. OUTLOOK

The work presented in the present study contributes to a better understanding of the functions of the different phases in selective oxidation catalysts.

The oxides we have investigated are the main components in many formulations of selective oxidation catalysts. Molybdenum plays an essential role in many such formulations. It adsorbs the hydrocarbon and incorporates the lattice oxygen into the product. Molybednum is always associated with other elements in selective oxidation catalyst. The catalytic system which has been most studied is bismuth molybdate. Bismuth is indeed believed to play an essential role in replenishing bismuth molybdate lattice in oxygen (*9, 47, 48*). Previous results obtained in the study of the dehydration of formamides have also indicated that Bi as

$BiPO_4$ (*1, 49*) or as Bi_2O_3 were gateways to oxygen. In the present case, α-Sb_2O_4 also replenishes MoO_3 in oxygen. Another group of investigators in our laboratory found a similar cooperative effect between α-Sb_2O_4 and MoO_3 for the oxidation of isobutene to methacrolein (*3, 44–46*). All these results suggest that Bi as well as Sb or other elements could play a similar role in multiphase catalysts containing Mo (or Fe, Sn, and U) when they work in selective oxidation.

Incidentally, our results may present an analogy with deactivation phenomena observed in selective oxidation. Our results could possibly lead to a better understanding of the reaction mechanism of selective oxidation on oxide catalysts. It is well established that in the case of selective oxidation, the lattice oxygen of catalysts takes part in the reaction, and the reduced catalyst is reoxidized by means of the replenishment of the oxygen vacancies with the oxygen species activated by an element near those vacancies (*11, 50–56*). Literature mentions the influence of cabon deposit on the activity of oxide catalysts. In particular, for the ammoxidation of propylene on Bi_2O_3 + MoO_3 catalysts in the absence of gaseous oxygen, the carbon deposit is proportional to the reaction time and, consequently, the nitrile yield decreases progressively (*57*).

All the analogies between the catalytic effects observed in our reaction and those occurring in selective oxidation lead us to the conclusion that the cooperative effect between two phases of many oxidation catalysts extensively studied in the literature, such as MoO_3 + Bi_2O_3 (*58, 59*), MoO_3 + Sb_2O_4 (*3*), MoO_3 + $BiPO_4$ (*49*), Sn_2O_4 + Sb_2O_4 (*60*), MoO_3 + $NiMoO_4$ (*15*), and $FeSbO_4$ + Sb_2O_4 (*18, 61, 62*) might also be explained partially or totally by the intervention of a remote control mechanism. Recent results (*63–69*) obtained in our laboratories seem to confirm this conclusion.

ACKNOWLEDGMENTS

The financial support of the Commissariat Général aux Relations Internationales de la Communauté Française de Belgique (B. Zhou) and the Service de Programmation de la Politique Scientifique (E. Sham, T. Machej, and P. Ruiz) is gratefully acknowledged. The ISS equipment was acquired thanks to a grant from the Fonds National pour la Recherche Scientifique of Belgium. We are indebted to Professor J. P. Bonnelle, Dr. O. B. Nagy, and Mr. M. Genet for their constructive discussions and comments.

REFERENCES

1. *a*. Tascon, J. M. D., Grange, P., and Delmon, B., *J. Catal.* **97,** 287 (1986).
   b. Tascon, J. M. D., Bertrand, P., Genet, M., and Delmon, B., *J. Catal.* **97,** 300 (1986).
   c. Tascon, J. M. D., Mestdagh, M. M., and Delmon, B., *J. Catal.* **97,** 312 (1986).
2. Zhou, B., Ceckiewicz, S., and Delmon, B., *J. Phys. Chem.* **91,** 5061 (1987).
3. Ruiz, P., Zhou, B., Remy, M., Machej, T., Aoun, F., Doumain, B., and Delmon, B., *Catal. Today* **1,** 181 (1987).
4. Zhou, B., Yasse, B., Doumain, B., Ruiz, P., and Delmon, B., *in* "Proceedings, 9th International Congress on Catalysis, Calgary, 1988" (M. J. Phillips and M. Ternan, Eds.), p. 1850. Chem. Institute of Canada, Ottawa, 1988.
5. Centi, G., and Trifiro, F., *Catal. Rev. Sci Eng.* **28,** 165 (1986).
6. Pitchai, R., and Klier, K., *Catal. Rev. Sci Eng.* **28,** 13 (1986).
7. Kung, H. H., *Ind. Eng. Chem. Prod. Res. Dev.* **25,** 171 (1986).
8. Kung, H. H., and Kung, M. C., *Adv. Catal.* **33,** 159 (1985).
9. Grasselli, R. K., and Burrington, J. D., *Adv. Catal.* **30,** 133 (1981).
10. Berry, F. J., *Adv. Catal.* **30,** 97 (1981).
11. Dadyburjor, D. B., Jewur, S. S., and Ruckenstein, E., *Catal. Rev. Sci. Eng.* **19,** 293 (1979).
12. Margolis, L. Ya., *Catal. Rev.* **8,** 241 (1973).
13. Voge, H. H., and Adams, Ch. R., *Adv. Catal.* **17,** 151 (1967).
14. Weng, L. T., Ruiz, P., Delmon, B., "III Europ Workshop Meeting: New Developments in Selective Oxidation, Louvain-la-Neuve, Belgium, April 8–10, 1991," preprints.
15. *a*. Ozkan, U., and Schrader, L. G., *J. Catal.* **95,** 120 (1985);
   b. Ozkan, U., and Schrader, L. G., *J. Catal.* **95,** 137 (1985);
   c. Ozkan, U., and Schrader, L. G., *J. Catal.* **95,** 147 (1985).
16. *a*. Moro-oka, Y., Tan, S., and Ozaki, A., *J. Catal.* **12,** 291 (1986);
   b. Moro-oka, Y., Tan, S., and Ozaki, A., *J. Catal.* **17,** 125 (1970);
   c. Moro-oka, Y., Tan, S., and Ozaki, A., *J. Catal.* **12,** 132 (1970).

17. Grzybowska, B., and Volta, J. C., *Appl. Catal.* **22,** 181 (1986).
18. Teller, R. G., Brazdil, J. F., Grasselli, R. K., and Yelon, W., *J. Chem. Soc. Faraday Trans.* **81,** 1693 (1985).
19. Centi, M. C. G., and Trifiro, F., *J. Catal.* **91,** 85 (1985).
20. Volta, J. C., Bussiere, P., Coudurier, G., Herrmann, J. M., and Vedrine, J. C., *J. Catal.* **16,** 315 (1985).
21. Boudeville, Y., Figueras, F., Fourissier, M., Portefaix, J. L., and Vedrine, J. C., *J. Catal.* **58,** 52 (1979).
22. Nassau, K., Levinstein, H. J., and Louicono, Gr., *J. Phys. Chem. Solids* **26,** 1805 (1965).
23. Nassau, K., Shiever, J. W., and Keve, E. T., *J. Solid State Chem.* **3,** 411 (1971).
24. Parmentier, M., Courtois, A., and Gleitzer, C., *Bull. Soc. Chim. Fr. 1,2* **75** (1974).
25. Parmentier, M., Gleitzer, C., and Tilley, R. J., *J. Solid State Chem.* **31,** 305 (1980).
26. Birchall, T., Connor, J. A., and Hiller, I. H., *J. Chem. Soc. Dalton Trans.* 2003 (1975).
27. Wachs, I. E., Chan, S. S., and Saleh, R. Y., *J. Catal.* **91,** 3 (1985).
28. Bond, G. C., Zurita, J. P., Flamerz, S., Gellings, P. J., Bosch, H. Van Ommen, J. G., and Kip, B. J., *Appl. Catal.* **22,** 361 (1986).
29. Sonnemans, J., and Mars, P., *J. Catal.* **31,** 209 (1978).
30. Bond, G. C., and Bruckman, K., *Faraday Discuss. Chem. Soc.* **72,** 235 (1981).
31. Gopalakrishnan, P. S., and Manohar, H., *Cryst. Struct. Comm.* **4,** 203 (1975).
32. Andersen, H. H., and Bay, H. L., *in* "Sputtering by Particle Bombardment I" (R. Behrisch, Ed.), Topics in Applied Physics, Vol. 47, p. 181. Springer–Verlag, Berlin–Heidelberg, 1981.
33. Betz, G., and Wehner G. K., *in* "Sputtering by Particle Bombardment II" (R. Behrisch, Ed.), Topics in Applied Physics, Vol. 52, p. 57. Springer-Verlag, Berlin-Heidelberg, 1983.
34. Jones, R. F., Gale, P., Hopkins, P., and Powell, L. N., *Analyst* **90,** 623 (1965).
35. Boudeville, U., Figueras, F., Forissier, M., Portefaix J. L., and Vedrine, J. C., *J. Catal.* **58,** 52 (1979).
36. Wagner, C. D., Riggs, W. M., Davis, L. E., Moulder, J. F., and Muilerberg, C. E. "Handbook of X-Ray Photoelectron Spectroscopy." Perkin–Elmer Corp., Minnesota, 1978.
37. Chin, R. L., and Hercules, D. M., *J. Phys. Chem.* **86,** 3079 (1982).
38. Petterson, T. A., Carver, J. C., Leyden, D. E., and Hercules D. M., *J. Phys. Chem.* **80,** 1700 (1976).
39. Teller, R. G., Antonio, M. R., Brazdil, J. F., Mehicic, M., and Grasselli, R. K., *Inorg. Chem.* **24,** 3370 (1985).
40. Teller, R. G., Antonio, M. R., Brazdil, J. F., Mehicic, M., and Grasselli, R. K., *J. Solid State Chem.* **64,** 249 (1986).
41. Birchall, T., Hallett, C., and Sleight, A. W., *J. Chem. Soc. Dalton Trans.* **853** (1986).
42. Bertrand, P., Beuken, J. M., and Delvaux, M., *Nucl. Instrum. Methods Phys. Res.* 218, 249 (1983).
43. Stampfle, S. R., Chen, Y., Dumesic, J. A., Niu, C. M., and Hill, C. G., Jr., *J. Catal.* **105,** 445 (1987).
44. Weng, L. T., Zhou, B., Yasse, B., Doumain, B., Ruiz, P., and Delmon, B., "Proceedings, 9th International Congress on Catalysis, Calgary, 1988" (M. J. Phillips and M. Ternan, Eds.), p. 1609, Chem. Institute of Canada, Ottawa, 1988.
45. Delmon, B., and Ruiz, P., *React. Kinet. Catal. Lett.* **35,** 303 (1987).
46. Ruiz, P., and Delmon, B., "194th ACS National Meeting, New Orleans, preprints"; *Petrol. Div.* **36** (1987); *Catal. Today* **3,** 199 (1988).
47. Grasselli, R. K., *Appl. Catal.* **15,** 127 (1985).
48. Gleser, L. C., Brazdil, J. F., Hazle, M. A., Mehicic, M., Grasselli, R. K., *J. Chem. Soc. Faraday Trans. 1* 81, 2903 (1985).
49. Rodriguez, M. V. E., Delmon, B., and Viehe, H. G., *Ind. Eng. Chem. Prod. Res. Dev.* **21,** 42 (1982).
50. Keulks, G. W., *J. Catal.* **19,** 232 (1970).
51. Wragg, R. V., Ashmmore, P. G., and Hockey, J. A., *J. Catal.* **22,** 49 (1971).
52. Haber, J., *in* "Proceedings, 8th International Congress on Catalysis, Berlin, 1984," p. I-85. Dechema, Frankfurt-am-Main, 1984.
53. Hucknall, D. J., "Selective Oxidation of Hydrocarbons," Academic Press, New York/London, 1974.
54. Schuit, C. C. A., *J. Less-Common Met.* **36,** 329 (1974).
55. Callahan, J. L., Grasselli, R. K., Milberger, E. C., and Strecher, H. A., *Ind. Eng. Chem. Prod. Res. Dev.* **9,** 134 (1970).
56. Brazdil, J. F., Suresh, D. D., and Grasselli, R. K., *J. Catal.* **66,** 387 (1980).
57. Aykan, K., *J. Catal.* **12,** 281 (1968).
58. Ceckiewicz, S., and Delmon, B., *Bull. Soc. Chim. Belg.* **93,** 163 (1984).
59. Hayakawa, T., Tsunoda, T., Orita, H., Kameyama, T., Takahashi, H., Fukuda, K., and Takahira, K., *J. Chem. Soc. Chem. Commun.* 780 (1987).
60. Weng, L. T., Spitaels, N., Yasse, B., Ladrière, J., Ruiz, P., and Delmon, B., submitted for publication.
61. Straguzzi, G. I., Bischoff, K. B., Koch, T. A., and Schuit, G. C. A., *Appl. Catal.* **25,** 257 (1987).
62. *a.* Straguzzi, G. I., Bischoff, K. B., Koch, T. A., and Schuit, G. C. A., *J. Catal.* **103,** 357 (1987); *b.* Straguzzi, G. I., Bischoff, K. B., Koch, T. A., and Schut, G. C. A., *J. Catal.* **104,** 47 (1987).

63. Patrono, P., Weng, L. T., Sham, E. L., Ruiz, P., and Delmon, B., "XI Simposio Iberoamericano de Catalisis, Guanajuato, Mexico, 12–17 junio, 1988," p. 911.
64. Weng, L. T., Spitaels, N., Yasse, B., Ladrière, J., Ruiz, P., and Delmon, B., ("XI Simposio Iberamericano de Catalisis, Guanajuanto, Mexico, 12–17 junio, 1988," p. 929.
65. Weng, L. T., Duprez, D., Ruiz, P., and Delmon, B., "XI Simposio Iberamericano de Catalisis, Guanajuanto, Mexico, 12–17 junio, 1988," p. 955.
66. Weng, L. T., Patrono, P., Sham, E. L., Ruiz, P., and Delmon, B., New Developments in Selective Oxidation, I. World Congress, II European Workshop Meeting, Rimini, Italy, September 19–22, 1989," p. 797.
67. Weng, L. T., Sham, E., Doumain, B., Ruiz, P., and "New Developments in Selective Oxidation, I. World Congress, II European Workshop Meeting, Rimini, Italy, September 19–22, 1989," p. 757.
68. Qiu, T. Y., Weng, L. T., Ruiz, P., and Delmon, B., "Second International Conference on Spillover, Leipzig, German Democratic Republic, June 12–16, 1989," p. 136.
69. Weng, L. T., Ruiz, P., Delmon, B., "Second International Conference on Spillover, Leipzig, German Democratic Republic, June 12–16, 1989," p. 37.